Numerical Model of Long-Lived Jovian Vortices

ANDREW P. INGERSOLL AND P. G. CUONG

Division of Geological and Planetary Sciences, California Institute of Technology, Pasadena 91125

(Manuscript received 12 January 1981, in final form 22 May 1981)

ABSTRACT

A nonlinear numerical model of long-lived Jovian vortices has been constructed. We assume that the measured zonal velocity profile $\bar{u}(y)$ extends into the adiabatic interior, but that the eddies and large oval structures are confined to a shallow stably stratified upper layer. Each vortex is stationary with respect to the shear flow $\bar{u}(y)$ at a critical latitude y_c that is close to the latitude of the vortex center, in agreement with observed flows on Jupiter. Our model differs from the solitary wave model of Maxworthy and Redekopp in that the stratification is not large in our model (the radius of deformation is less than the latitudinal scale of the shear flow), and therefore stationary linear wave solutions, neutral or amplified, do not exist. The solutions obtained are strongly nonlinear in contrast to the solitary wave solutions which are the weakly nonlinear extensions of ultralong linear waves. Both stable and unstable vortices are found in the numerical experiments. When two stable vortices collide, they merge after a short transient phase to form a larger stable vortex. This merging, rather than the non-interaction behavior predicted by the solitary wave theory, is more in agreement with observations of Jovian vortices. We suggest that the long-lived Jovian vortices maintain themselves against dissipation by adsorbing smaller vortices which are produced by convection.

1. Introduction

The Great Red Spot (GRS) on Jupiter has been observed for at least 100 years. Various models have been constructed in order to explain this striking phenomenon. The hypothesis of a deep-rooted Taylor column (Hide, 1963; Ingersoll, 1969) has long been disregarded due to the observed longitudinal variations of the GRS with respect to the Jovian magnetic field, and also to the doubtful existence of any solid surface in the Jovian interior.

Ingersoll (1973) suggested that the GRS might be identified as a steady-state unforced flow obeying the barotropic vorticity equation. Steady, closed-streamline solutions resembling observed Jovian flows were found numerically, but only in a narrow channel between latitudinal barriers.

Maxworthy and Redekopp (1976, hereinafter referred to as MR) suggested that the GRS and other Jovian spots are manifestations of solitary Rossby waves (see also Redekopp, 1977). Closed streamline flows resembling observed Jovian flows were obtained analytically, assuming a weakly nonlinear, long-wavelength disturbance on a parallel zonal flow. For barotropic flows, such solutions again were obtained only in a narrow channel. For baroclinic flows with stratification, solutions were obtained without latitudinal barriers. The effect of stratification is to make ultralong, stationary, linear neutral waves possible. The governing nonlinear equation for the amplitude exhibits soliton behavior, i.e., disturbances pass through each other with no net interaction.

The present model resembles the baroclinic model of MR in some respects. The basic equation is identical to theirs, and is here derived for a hydrostatic, quasi-geostrophic two-layer model in which the lower layer is much deeper than the upper layer. Flow in the lower layer is unaffected by motion in the upper layer, and is assumed to be a parallel shear flow $\bar{u}(y)$ with maximum profile radius of curvature L. Flow in the upper layer includes isolated, closed streamline regions that tend toward the lower layer flow $\bar{u}(y)$ in a horizontal distance equal to the radius of deformation. The chief difference between our work and MR is that the stratification is now not large, so the radius of deformation L_D is also not large. Thus, $k^2 \equiv L^2/L_D^2$ is greater than one in our model. The influence of the lower layer shear flow $\bar{u}(y)$ on the upper layer dynamics is strong. Stationary, linear neutral and amplifying solutions now do not exist in the upper layer, so a weakly nonlinear, solitary wave solution is impossible. Thus the closed-streamline solutions that we have found numerically do not exhibit soliton behavior. Rather, vortices tend to merge and form a stronger new vortex.

Since the flow is inviscid and adiabatic in our model, the important questions are ones of stability. We will not discuss the stability of the lower layer shear flow $\bar{u}(y)$. Both in our model, in MR and on Jupiter the basic flow $\bar{u}(y)$ violates the barotropic

0022-4928/81/102067-10$06.50

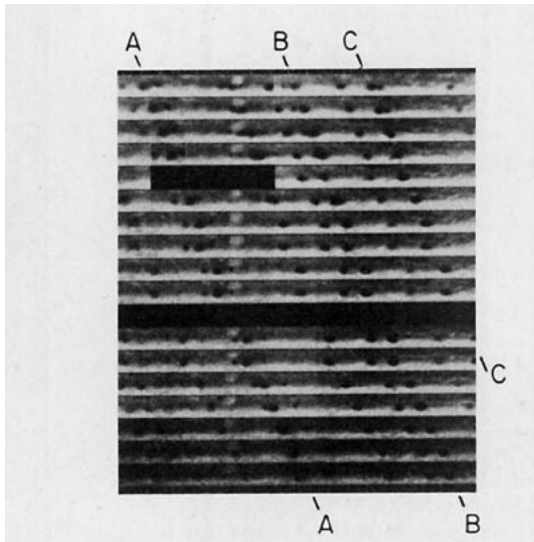

FIG. 1. Time lapse sequence of spot interactions centered at Jovian latitudes of 34°. Each strip is from a Mercator projection of Voyager 1 images, and covers 10 000 km in the north-south direction. The strips are separated in time by four Jovian rotations (~40 h), with time increasing downward and east to the right. Irregularities in longitudinal position result from errors in registering the original images. Three groups of spots (A, B, C) for which merging takes place may be followed. The sequence was prepared at the Image Processing Laboratory, Jet Propulsion Laboratory, as part of the Voyager project.

stability criterion. The dynamics of the lower region will be discussed in future papers. Here we merely assume that the lower layer is deep and adiabatic, so that it is unaffected by upper layer motions. The stability of the upper layer flow will be addressed in two ways. First, we will consider a basic state in which the upper layer moves with the lower layer shear flow $\bar{u}(y)$. For $k^2 < 1$, as in MR, this upper layer flow is unstable. For $k^2 > 1$, as in the present paper, this flow is stable. A deficiency of MR is that the finite-wavelength, unstable modes are left out of their theory; only the ultralong, neutral mode and its nonlinear interactions are treated. Second and most important, we will consider the stability of the vortices themselves. By nonlinear iteration, we can create steady solutions for the upper layer flow that tend, in one radius of deformation, to the lower layer solution $\bar{u}(y)$, but which have isolated closed streamline regions that move with the flow. Their stability is tested by perturbing and integrating forward in time. Both small- and large-amplitude perturbations are studied. An example of the latter occurs when two vortices collide and merge.

2. Observational constraints and assumptions

Here we briefly review pertinent observations of Jupiter, many obtained during the 1979 Voyager encounters. The basic shear flow $\bar{u}(y)$ has been steady in time for at least 80 years (Smith and Hunt, 1976; Ingersoll *et al.*, 1981). The root-mean-square (rms) amplitude (averaged with respect to latitude) of $\bar{u}(y)$ is about 50 m s^{-1}. The relative vorticity gradient $\bar{u}_{yy}$ varies with latitude in the range -3β to $+2\beta$, where β is the planetary vorticity gradient (Ingersoll *et al.*, 1981). The kinetic energy transfer $\{K'\bar{K}\}$ from eddies to mean flow is of order 2×10^{-4} m^2 s^{-3}, which is sufficient to double the zonal mean kinetic energy in about 75 earth days, assuming the eddies and the mean flow are confined to the same atmospheric layer (Beebe *et al.*, 1980; Ingersoll *et al.*, 1981). Existing wind measurements do not define the scale of eddies contributing to this energy transfer, although movies and single images suggest a dominant eddy radius in the range 200 to 1000 km. The rms eddy velocities are of order 10–20 m s^{-1} (Ingersoll *et al.*, 1981). These small transient eddies typically appear as bright convective elements at latitudes of strong cyclonic shear, where they are pulled apart in times of order 1–2 days (Ingersoll *et al.*, 1979; Mitchell *et al.*, 1979).

In contrast, the larger eddies tend to be long-lived, physically isolated, anticyclonic, and oval-shaped. Their edges appear sharp. That is, the transition of cloud color and type occurs in distances < 1000 km, which is an order of magnitude less than the size of these oval features. They sit in anticyclonic shear zones and move at an intermediate speed between the maximum eastward and maximum westward currents. Each vortex is therefore stationary with respect to the flow at some critical latitude. The GRS and the three white ovals have peak vorticities that are four times that of the ambient shear and one-third to one-half the local planetary vorticity (Mitchell *et al.*, 1979, 1981). The planetary vorticity difference from north to south across these spots is comparable to the peak relative vorticity. Smaller spots approaching the GRS are accelerated around it and often merge with it (Smith *et al.*, 1979a, Fig. 8). Spots of equal size also merge, sometimes ejecting material before settling down to a new equilibrium (Smith *et al.*, 1979a, Fig. 9; Smith *et al.*, 1979b, Fig. 7). Merging was observed from earth before Voyager (Reese and Smith 1968, Fig. 7). The acceleration of spots that pass each other but do not merge also was observed from earth (Reese, 1970; Smith and Hunt, 1976) as emphasized by MR. A further example of merging is shown in Fig. 1.

The vertical structure of these features is still uncertain. Significant latent heat release, absorption of sunlight, and emission to space all occur in a layer 1–3 scale heights (30–100 km) thick near the level of the visible clouds. Various authors (Ingersoll and Cuzzi, 1969; Barcilon and Gierarch, 1970; Stone, 1972; Maxworthy and Redekopp, 1976; Williams, 1978, 1979) have assumed that the atmosphere below this cloud zone is in solid-body rotation, or else has no effect on the motions in the clouds. In particular,

Williams (1978, 1979) has had considerable success producing realistic zonal flows from baroclinic eddies via the $\{K'\bar{K}\}$ term. His model is basically a terrestrial two-layer model scaled for Jupiter's cloud zone, with a solid surface at the lower boundary. Large, oval gyres appear in his numerical experiments, but these are mostly periodic in x, unlike the more isolated Jovian spots. The largest such structure (the Gyre) fills its periodic integration domain in x, and is thus a normal mode rather than an isolated vortex.

Despite Williams' success in producing zonal flows in a shallow layer, we are inclined to favor a model in which the zonal flow $\bar{u}(y)$ extends much deeper than the eddies, perhaps a significant fraction of the planetary radius. The steadiness of the zonal flow over 80 years, despite the large $\{K'\bar{K}\}$ term, argues in favor of such a model. The zonal flow would then possess much more inertia than the eddy flow in the visible clouds, and the time constant for changing $\bar{u}(y)$ would then be much longer than the 75-day estimate given earlier. Also, the dynamics of rapidly rotating, adiabatic fluids argues in favor of such a model. For a given horizontal scale, the depth to which the flow features extend is limited only by departures from adiabaticity, by friction, or by variations with time. Since these effects are all likely to be small below the cloud zone (Gierasch *et al.*, 1979), the steady flow $\bar{u}(y)$ could extend to great depths.

The arguments of the preceding paragraph are not conclusive. Nevertheless, we proceed on the assumption that the basic shear flow $\bar{u}(y)$ exists in the adiabatic fluid interior of Jupiter, and that the long-lived eddies are confined to a less dense upper layer which we associate with the cloud zone. The radius of deformation L_D for the upper layer is then of order $(R\Delta\theta/f^2)^{1/2}$, where R is the gas constant for a hydrogen-helium mixture, $\Delta\theta$ the potential temperature difference between upper and lower layers, and f the Coriolis parameter. Taking $R = 3.7 \times 10^3$ J kg^{-1} K^{-1}, $\Delta\theta = 2$ K, $f = 1.75 \times 10^{-4}$ s^{-1}, we obtain $L_D = 500$ km. This value of $\Delta\theta$ is the approximate temperature change associated with latent heat release (Barcilon and Gierasch, 1970). At the opposite extreme, taking $\Delta\theta \approx \theta \approx 200$ K, we obtain $L_D = 5000$ km. Even the latter value is smaller than the 10 000 km semi-major axis of the GRS, and comparable to the semi-major axis of the white ovals. Thus our second important assumption is that the radius of deformation is comparable to or smaller than the horizontal scale L of the shear flow and of the long-lived vortices.

We do not expect a direct observational test of these assumptions in the near future. Support for the theory comes from the extent to which it accounts for the appearance and time-dependent behavior of these long-lived vortices. Improvements in the theory can be expected by having more than one vertical degree of freedom, by including energy sources and sinks, and by understanding the dynamics of Jupiter's fluid interior.

3. Mathematical formulation

For simplicity the fluid is assumed to be incompressible, with densities ρ_1 and ρ_2 in the upper and lower layers, respectively, such that $\rho_2 > \rho_1$. The flow is inviscid, with no external forces other than gravity. The hydrostatic, quasi-geostrophic and β-plane approximations are used. At the upper free surface the pressure P is zero. At the free interface between the two fluids the pressure is continuous and equal to $\rho_1 gH$, where $H(x, y, t)$ is the thickness of the upper layer and g is the acceleration of gravity. The geostrophic approximation implies that horizontal velocities are computed from the gradient of a streamfunction ψ, i.e.,

$$\left.\begin{aligned} u_n(x, y, t) &= -\frac{\partial \psi_n}{\partial y} = -\frac{1}{\rho_n f_0}\frac{\partial P_n}{\partial y} \\ v_n(x, y, t) &= \frac{\partial \psi_n}{\partial x} = \frac{1}{\rho_n f_0}\frac{\partial P_n}{\partial x} \end{aligned}\right\}. \quad (1)$$

Here $n = 1$ or 2 for the upper and lower layers, respectively. The eastward and northward velocities are u_n and v_n, with corresponding coordinates x and y. The Coriolis parameter at the mean latitude of the β-plane is f_0, and we use the approximation

$$f(y) = 2\Omega \sin\theta \approx f_0 + \beta y, \quad (2)$$

where θ is latitude and Ω the planetary rotation rate. With these approximations, the upper layer thickness $H(x, y, t)$ can be related to the streamfunctions ψ_1 and ψ_2 as

$$H(x, y, t) = H_0 + \left(\frac{\rho_2}{\rho_2 - \rho_1}\right)\frac{f_0}{g}(\psi_1 - \psi_2). \quad (3)$$

Here H_0 is the undisturbed thickness of the upper layer, corresponding to $\psi_1 = \psi_2 = 0$.

The dynamical equation governing the flow in each layer is conservation of potential vorticity (e.g., Holton, 1979; Pedlosky, 1979). For the upper layer this implies

$$\frac{d}{dt}\left(\frac{\nabla^2\psi_1 + f}{H}\right) = 0, \quad (4)$$

where d/dt is the total time derivative. Eq. (4) is not exact only because we use the geostrophic expression $\nabla^2\psi_1$ for the vorticity. Fractional changes in the thickness H need not be small provided the flow is approximately parallel to constant thickness contours. However, because of the great thickness of the lower layer, changes in the interface height and hence in the motion of the upper layer are negligible as far as lower layer dynamics are con-

cerned. Our basic assumption is therefore that the lower layer streamfunction is

$$\psi_2(y) = -\int \bar{u}(y)dy, \tag{5}$$

where $\bar{u}(y)$ is given.

We now introduce dimensionless variables, scaling all lengths and velocities by L and U, which are characteristic of the basic shear flow. The streamfunctions ψ_1 and ψ_2 are scaled by UL, and are written in dimensionless form as ψ and $\bar{\psi}$. The Rossby number ϵ is U/f_0L, and the dimensionless term β is $b = \beta L^2/U$. Finally, the dimensionless stratification parameter is k^{-2}, given by

$$k^{-2} = \frac{gH_0(\rho_2 - \rho_1)}{f_0^2L^2\rho_2} = \frac{L_D^2}{L^2}, \tag{6}$$

where L_D is the radius of deformation. With these definitions and assumptions the equation for the upper layer streamfunction $\psi(x, y, t)$ is

$$\left(\frac{\partial}{\partial t} + \frac{\partial\psi}{\partial x}\frac{\partial}{\partial y} - \frac{\partial\psi}{\partial y}\frac{\partial}{\partial x}\right) \times \left[\frac{1 + \epsilon\nabla^2\psi + \epsilon by}{1 + \epsilon k^2(\psi - \bar{\psi})}\right] = 0. \tag{7}$$

We have chosen to treat $k^2 \geq 1$ and $\epsilon \ll 1$, such that $\epsilon k^2 \ll 1$, where Eq. (7) becomes

$$\left(\frac{\partial}{\partial t} + \frac{\partial\psi}{\partial x}\frac{\partial}{\partial y} - \frac{\partial\psi}{\partial y}\frac{\partial}{\partial x}\right) \times (\nabla^2\psi + by - k^2\psi + k^2\bar{\psi}) = 0. \tag{8}$$

Boundary conditions are that $\partial\psi/\partial x$ vanish at the north-south boundaries y_1 and y_2, and that ψ be periodic in x. The region of integration is meant to be large compared to L.

Eq. (8) is symmetric with respect to cyclonic versus anticyclonic vortices, although (7) is not. This symmetry with respect to the sign of the vorticity is not found on Jupiter, where long-lived vortices are predominantly anticyclonic (but see Hatzes *et al.*, 1981). One possibility is that finite displacements of the thickness H are occurring, for which Eqs. (4) and (7) are the appropriate equations instead of (8).

For comparison with MR, it is useful to linearize equation (8) about a basic state in which the upper layer moves with the lower layer shear flow $\bar{u}(y)$. Thus $\psi = \bar{\psi} + \varphi$, $|\varphi| \ll |\bar{\psi}|$, and we have

$$\nabla^2\varphi - k^2\varphi + \left(\frac{b - \bar{u}_{yy}}{\bar{u} - c}\right)\varphi = 0. \tag{9}$$

Here c is the phase speed of the disturbance and $\bar{u}$ is now dimensionless. Eq. (9) might describe either a linear wave in x superposed on the shear flow $\bar{u}(y)$ or else the far-field generated by a nonlinear vortex moving with real velocity c. For Jupiter, the case of interest has $-1 < c < 1$, corresponding to a steady disturbance moving at an intermediate speed relative to the shear flow. A necessary condition for regular neutral solutions of (9) is that the bracketed coefficient be analytic, i.e., that $b - \bar{u}_{yy}$ change sign at latitudes where $\bar{u}(y) = c$. For Jupiter, the condition $b - \bar{u}_{yy} = 0$ ($\beta = \bar{u}_{yy}$ in dimensional notation) is met at many latitudes, and these latitudes are approximately where one finds the large, long-lived vortices.

We depart company with MR at this point. They base their solution on the ultra-long linear waves in x, whence they require $k^2 \leq 1$ in order that Eq. (9) give oscillatory behavior. Our solution is inherently nonlinear, and we require $k^2 \geq 1$ in order that the far-field of the vortex decay exponentially to zero. In our model, therefore, the upper layer flow tends to the lower layer shear at distances greater than one radius of deformation. As an example, consider the dimensionless profile

$$\bar{u}(y) = \cos y, \quad b < 1. \tag{10}$$

Regular neutral solutions with $-1 < c < 1$ then imply $c = -b$, where $-1 < c < 0$ and $b < 1$. In dimensional notation these conditions imply $\bar{u}_{\min} < c < \bar{u}_{\text{avg}}$ and $\beta < (\bar{u}_{yy})_{\max}$. Eq. (9) is then

$$\nabla^2\varphi - (k^2 - 1)\varphi = 0. \tag{11}$$

The solution is wavelike or exponential as k^2 is either less than or greater than 1. Notice that the decay length becomes equal to the radius of deformation L_D as k^2 becomes larger than 1. This exponential decay of the solution with horizontal distance away from the vortex is a special property of our model. If the shear flow $\bar{u}(y)$ were confined to the upper layer with the deep lower layer at rest such that $\bar{\psi} = 0$ in (8), the relevant equation would be $\nabla^2\varphi + \varphi = 0$ instead of (11). Likewise if there were only one barotropic layer with flat, rigid boundaries at top and bottom, the relevant equation also would be $\nabla^2\varphi + \varphi = 0$. In these cases the solution would be wavelike and not exponential.

Eq. (9) has been extensively studied by Kuo (1949), Lipps (1965) and others. When $k^2 < 1$, such that a regular neutral solution exists, then the upper layer flow is unstable. That is, complex eigenvalues of c have solutions φ that satisfy the boundary conditions. Growth rates are of order U/L and wavelengths are of order L. Comparing solutions of Eqs. (8) and (9) provides a good test of our numerical approach. An example is discussed briefly in Section 5. When $k^2 > 1$, we find no evidence of instability for the upper layer flow.

4. Numerical approach

In general our method is to use a nonlinear iteration scheme to obtain an initial state which can be either steady or not. The evolution of such a state is

then studied by time integration. The dependent variable $\psi(x, y, t)$ is computed on a Cartesian grid in x and y. Eq. (8) is integrated using centered time differences, with a forward integration every 50 time steps. Arakawa's (1966) nonlinear advection scheme is used to ensure conservation of energy and mean-squared vorticity. Poisson's equation is solved by means of a fast Fourier transform in x followed by Gaussian elimination in y. Tests were run to verify that the solution was independent of the grid spacing Δx, the time step Δt, and the location of the boundaries. Typically, solutions were obtained on a 64×64 grid, with $\Delta x = 3\pi/64$ and $\Delta t = 0.4\ \Delta x$.

For a vortex that is steadily moving with velocity c, we have $\psi = \psi(x - ct, y)$. Eq. (8) then implies

$$\nabla^2\psi + by - k^2\psi + k^2\bar{\psi} = F(\psi + cy), \quad (12)$$

where F is an arbitrary function of integration. For an isolated vortex, the streamfunction ψ approaches $\bar{\psi}$ in the far field. For the sinusoidal velocity profile equation (10) with $c = -b$, this implies $F(\psi') = -\psi'$, where $\psi' = \psi + cy$ is the streamfunction in the moving reference frame. The equation for ψ' is then

$$\nabla^2\psi' - (k^2 - 1)\psi' = -k^2\bar{\psi} - (k^2 - 1)cy, \quad (13)$$

which is valid everywhere outside closed-streamline regions. Eq. (13) is identical to (11), but is not restricted to the far-field or to small perturbations.

We produce a vortex by letting F be a different linear function of ψ' on closed streamlines. Adjusting both the derivative and the constant term, we can fix the value of F at the center and also ensure continuity of F at the outer edge of the closed-streamline region. The derivative of F is discontinuous. We also are free to choose the closed streamline on which to impose this discontinuity. This nonanalytic property places our solution in a broad class of isolated structures (Flierl *et al.*, 1980) called modons after the first oceanographic example (Stern, 1975). To get steady solutions, the sign of F at the vortex center has to be opposite the sign of ψ, that is, negative for anticyclonic vortices and positive for cyclonic vortices. The discontinuity of $dF/d\psi$ was either imposed at the critical streamline (shown dashed in the figures) or on a streamline up to half way inside the vortex.

Having chosen the function $F(\psi')$, we solve Eq. (12) by iteration. An initial streamfunction $\psi'(x, y)$ is created with the right topography (a central peak or depression with ridges and troughs representing the zonal flow). The computer locates the closed and open streamlines, and then evaluates the function $F[\psi'(x, y)]$ at each grid point. The left side of (12) is then inverted for a new $\psi'(x, y)$, and the iteration proceeds. Terms proportional to ψ' may be added to both sides of (12) to hasten convergence. For example, the left-side operator of Eq. (12) was often made equal to the left side of (13). Usually the iteration converged completely in 20 steps. Sometimes the iteration was stopped before it had converged, e.g., after ≤ 5 steps. In either case, the solution obtained could then be introduced as the initial streamfunction in a time integration of (8). Converged solutions are solutions of (12), and are therefore steady in the moving reference frame. They are not necessarily stable, however. Unconverged solutions are initially unsteady, although they often settle down to a steady, stable configuration rather quickly. Other unconverged solutions are unstable. Examples are given in the next section.

5. Results: Stability

In Figs. 2–7 we give contour maps of the upper layer streamfunction. The horizontal scale is compressed to 5% of the vertical scale. Time is measured in units of L/U, which we call days. Peak values of $d\bar{u}/dy$ on Jupiter suggest $L/U \approx 1$ to 2 Jovian rotations over much of the planet. The lower layer velocity profile is sinusoidal, i.e., Eq. (10) with $b = 0.3$. In dimensional units this corresponds to peak values for $\bar{u}_{yy}$ of $\pm\beta/0.3$. The streamlines are plotted in a reference frame moving westward at speed $|c| = b = 0.3$. The basic velocity in this frame is $\bar{u} - c$ which is shown in Fig. 3. It has the property that $b - \bar{u}_{yy} = 0$ at latitudes where $\bar{u} = c$.

We first discuss the stability of the basic shear flow $\bar{u}(y)$ in the upper layer. Here the upper layer flow is initially equal to the lower layer flow plus a small perturbation. The perturbation $\varphi = \hat{\varphi}(y)e^{i\alpha(x-ct)}$ obeys Eq. (9), therefore,

$$\frac{d^2\hat{\varphi}}{dy^2} - (k^2 + \alpha^2)\hat{\varphi} + \left(\frac{b - \bar{u}_{yy}}{\bar{u} - c}\right)\hat{\varphi} = 0, \quad (14)$$

with $\hat{\varphi}(y_1) = \hat{\varphi}(y_2) = 0$. For the sinusoidal velocity profile, it can be shown that equation (14) admits no stationary regular solutions unless

$$k^2 + \alpha^2 \leq 1 - \frac{n^2\pi^2}{|y_2 - y_1|}, \quad n = 1, 2, \cdots. \quad (15)$$

With $k^2 > 1$ this condition cannot be satisfied. However, it does not immediately follow that the flow is stable for $k^2 > 1$, since there might be a family of solutions with $c = c_r + ic_i$ such that c_i is always positive definite. To test for this, we solved Eq. (14) by a Runge-Kutta scheme with given values of $k^2 + \alpha^2$ for the complex eigenvalue c. This procedure is justified for amplified waves with c_i positive definite (Lin, 1955). We find no amplified solutions for $k^2 + \alpha^2 > 1$, and conclude that the shear flow is stable for $k^2 > 1$. This is confirmed by numerous time integrations of (8) in which the shear flow is perturbed but always remains stable for $k^2 > 1$. These results are consistent with Fig. 6 of Kuo (1949), for example, showing $c_i < 0$ at short wavelengths (large $k^2 + \alpha^2$ in our problem).

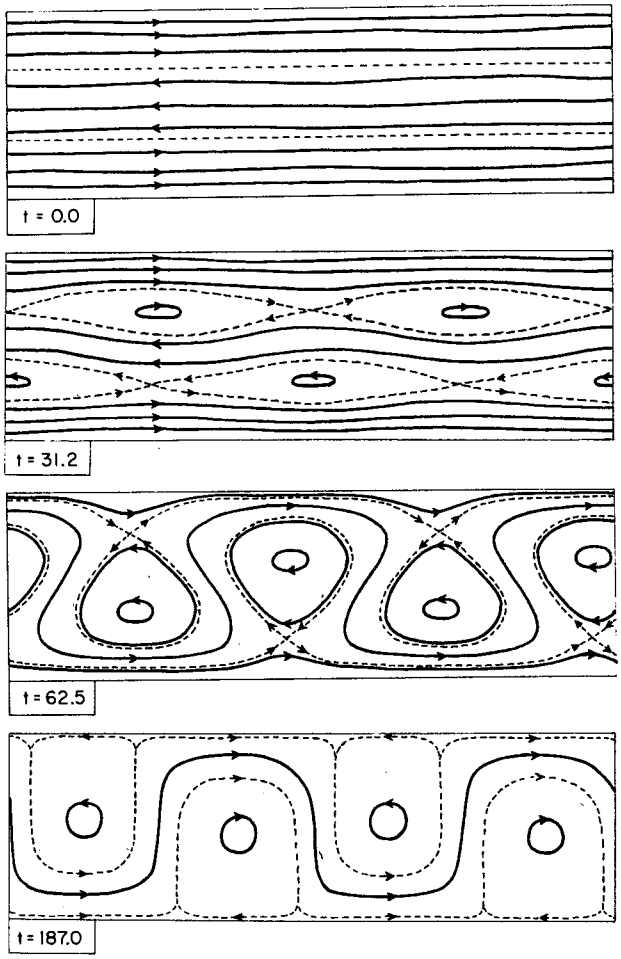

FIG. 2. Instability of $\bar{u} = \cos y$, with $y_1 = 0$, $y_2 = 2\pi$ for $k^2 = 0$. In Figs. 2–7 the x axis is compressed, such that a unit length appears ⅝ as long in the horizontal direction as in the vertical direction. Solutions are obtained on a 64 × 64 grid. The dashed lines represent the critical streamlines; the shapes near the cusps are uncertain.

For $k^2 < 1$ both neutral and amplified solutions exist. In this case we superpose the shear flow with the eigensolution of Eq. (14) that has the largest value of αc_i and start integrating in time. The shear flow becomes unstable at exactly the predicted rate, and is finally replaced by the wave pattern of the perturbation, as shown in Fig. 2. Since the flow must be periodic in x, the extent of the region in this direction must be equal to $n2\pi/\alpha$. Fig. 2 corresponds to $n = 2$ and $\alpha = 0.5$.

Returning to the case $k^2 > 1$, we next discuss nonlinear vortex solutions and their stability. An important quantity is P/K, the ratio of eddy potential energy to eddy kinetic energy. Here

$$\frac{P}{K} = \frac{\langle k^2(\psi - \tilde{\psi})^2 \rangle}{\langle (\partial\psi/\partial x)^2 + (\partial\psi/\partial y - \partial\tilde{\psi}/\partial y)^2 \rangle}, \quad (16)$$

where the tilde denotes an average with respect to x, and angle brackets denote an average over the whole domain. In general, we find that vortices with this ratio near unity are stable. When perturbed, or when started out without a fully converged solution of (12), they usually find a steady configuration by time $t = 20$ days.

Fig. 3 shows a stable solution after a long time integration, $t = 150$ days, during which no changes occurred. The value of P/K here is 1.05. The compactness of this vortex [cf. Eq. (11) and discussion following it] is due to the rather large value of $k^2 = 10$. For the same k^2, we find equally stable vortices with P/K equal to 1.60 and 2.18. Since the edges of Jovian vortices are sharp to within 1000 km, we conclude that the appropriate k^2 is large, such that the radius of deformation L_D is $\leqslant$1000 km. The solitary wave solutions of MR have $k^2 < 1$ and correspondingly long wavelength in x.

The stability of the solution changes completely for $P/K = 4.74$. This case is shown in Fig. 4, with k^2 still equal to 10. The original vortex is completely sheared apart by the basic flow after about 10 days. In cases similar to this one the presence of latitudinal barriers at finite distances from the original vortex do have some effect upon the solutions. These effects are manifestated by the off-and-on appearance of several vortices, of about the same strength (peak velocities) but much smaller in size in comparison with the initial vortex. Such appearance is due to the boundary reflection of disturbances which are created in the shearing of the original vortex and which cannot be dissipated away because of the inviscid nature of the problem.

For $k^2 = 5$, the initial vortices with $P/K = 2.95$, 2.07 and 1.74, respectively, exhibit the same unstable behavior. One interesting feature concerning this kind of instability is that in all these four cases it takes almost the same amount of time, which is about five days, for the initial total eddy energy to decrease by a factor of e. This suggests that these vortices are unstable due to the same mode of disturbance, i.e., same growth rate and wavelength.

For the same $k^2 = 5$ but with initial $P/K = 1.40$ the vortex seems to be unstable at first, but it steadies itself after a time $t = 6$ days. Similar behavior also occurs for initial vortices with $k^2 = 10$, $P/K = 0.56$ and $k^2 = 3$, $P/K = 1.07$. Both take about the same amount of time, $t = 6$ days, to recover themselves. To show that the vortex is most stable when P/K is closest to unity we take the case $k^2 = 3$. The initial vortices have P/K equal to 1.30, 1.15, 0.97, 0.74, respectively, and the corresponding times they spend to regain their stability are 9, 7, 3 and 5 days.

A common feature of all these cases of steadying vortices is that the vortices eject small disturbances, usually westward and equatorward. By this mechanism they seem to change their initial slightly unstable values of P/K to more stable values. Yet this is not easy to confirm, since at later times P/K

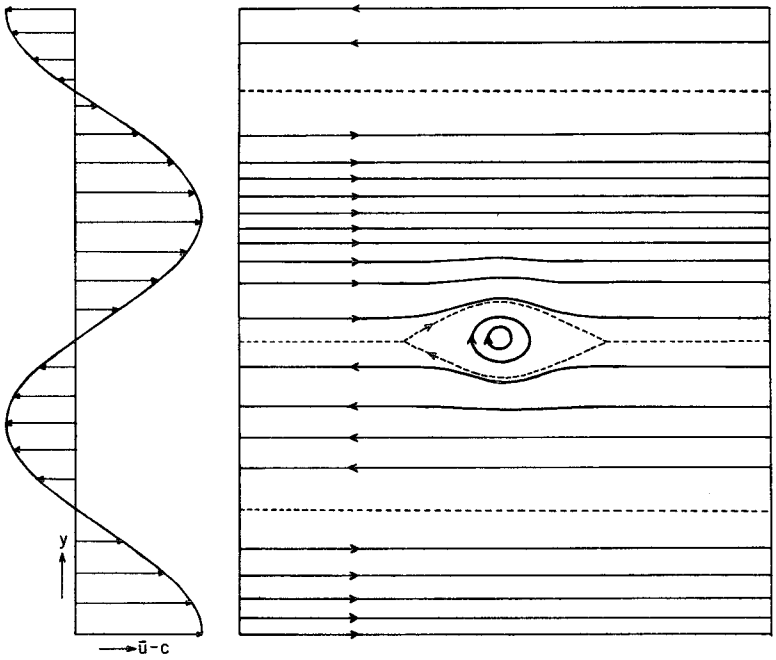

FIG. 3. On the left is the basic shear profile $\bar{u} = \cos y$, $y_1 = 0$, $y_2 = 3\pi$. The phase velocity of the wave is $c = -b = -0.3$. This profile is also used to obtain results shown in Figs. 4–7, although only the parts corresponding to $0.95\pi \leq y \leq 1.85\pi$ are plotted. On the right is the stable solution for $k^2 = 10$, $P/K = 1.05$.

includes contributions of the ejected disturbances, in addition to the main vortex. Fig. 5 gives an example of these steadying solutions.

At the smallest initial values of P/K, depending also on k^2, the vortex has to eject so much material in order to stabilize itself that it loses its identity completely. Such a vortex is eventually broken up into much smaller vortices which remain floating about in the basic flow. Such a case is shown in Fig. 6, with an initial $P/K = 0.23$.

We do not fully understand why the vortices are stable for P/K close to one. Nor have we varied all parameters $b, k^2, c, P/K, F(\psi')$, etc., in an exhaustive way to map out the stability field. For one mode of instability (e.g., Fig. 4), our results suggest that the size of the region (the vortex) in which the disturbance fits must be at least equal to L_D. This statement is roughly equivalent to the statement $P/K \geq O(1)$ for instability. For instability with $P/K < 1$ (Fig. 6), we have no simple explanations. We note that the sizes (relative to L) and peak vorticities (relative to U/L) of our numerical vortices are comparable to those of the three white ovals on Jupiter.

6. Results: Collisions

Our final topic concerns interactions between vortices. We are able to create pairs of vortices whose members have different velocities and sizes. Initially, the two vortices of a pair are located longitudinally far apart and at slightly different latitudes. Usually, for simplicity, one of them is at the latitude where $\bar{u} = c$, so that it is stationary in the reference frame of the figure, while the other is moving toward it either from the west or from the east.

According to (9), the far-field should be singular for any disturbance that is not moving at a velocity c such that $\bar{u} = c$, where $b = \bar{u}_{yy}$. However, we find no difficulty creating stable vortices that move at other speeds. Presumably, the singularity is not evident in our numerical solutions of equation (8) because one of the assumptions from which equation (9) was derived is violated. Thus the far-field may be slightly nonlinear at latitudes where $\bar{u}(y) \approx c$ or the flow may be slightly transient even in the reference frame moving with the vortex. It is perhaps surprising that these nonlinear and/or transient effects are so hard to see in our numerical integrations.

When the separation of their centers becomes less than the sum of their semiminor axes, the vortices interact. We find no evidence of the soliton-like interaction which characterizes MR's solitary-wave solutions. This should be expected because, for $k^2 > 1$, our solutions bear little connection with those of MR. We find, instead, that the colliding vortices always merge, forming a stable bigger vortex after a short transition phase. During this

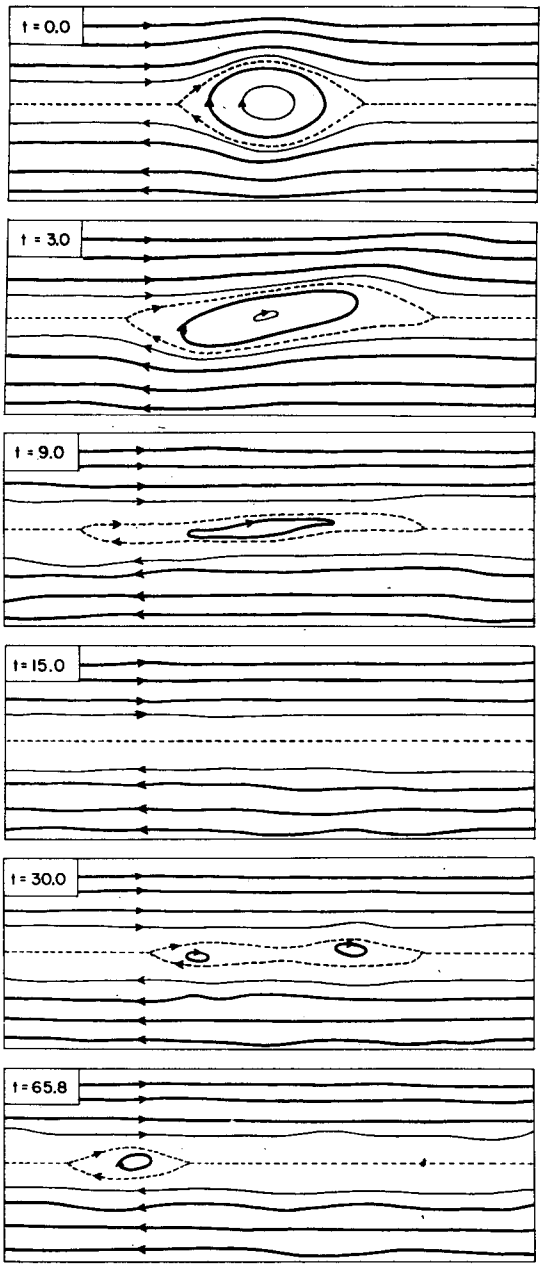

FIG. 4. An unstable solution for $k^2 = 10$, $P/K = 4.70$.

phase, small disturbances are ejected westward and equatorward. This particular behavior, according to the previous discussion concerning the stability of the vortices, suggests that the merging of two stable vortices usually results in a slightly unstable vortex which, in order to stabilize itself, resorts to the ejecting mechanism.

Fig. 7 shows two successive interactions of vortices. The first interaction is between two vortices of equal size while the one that follows concerns two of different sizes which are created as a result of the first interaction. Here, at $t = 0$, the vortex on the left is moving toward the one on the right, which is stationary with respect to the figure. At $t = 22.5$ the merging of the two takes place. This part of the figure shows a big, newly formed vortex which is stabilizing itself by ejecting a small vortex on its west side. At $t = 31.5$ both of them obviously become new stable vortices with their normal oval structures. The big one is now moving toward the east because its latitude is about the average of the latitudes of the two original vortices. The small one, being ejected slightly toward the equator, is at a latitude where $\bar{u} - c < 0$, and therefore is moving toward the west.

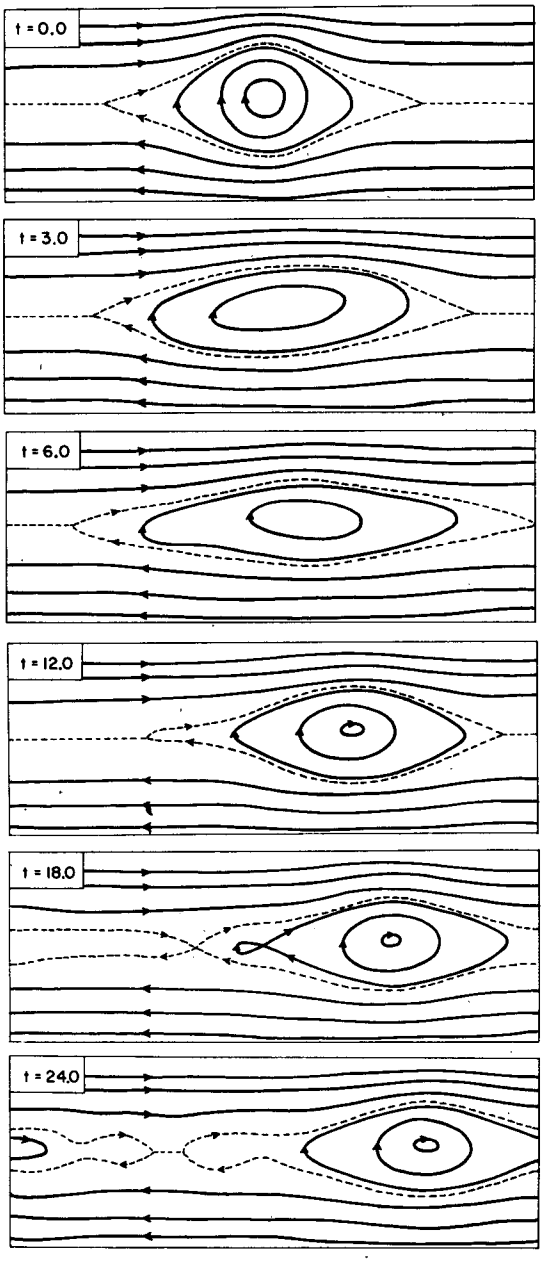

FIG. 5. A steadying solution for $k^2 = 3$, $P/K = 1.30$.

Because of the periodicity in x the new situation becomes one in which two stable vortices of different sizes will be colliding. This second collision occurs on the east side of the big vortex. The plot at $t = 44.8$ shows what happens a short time after the interaction. One sees clearly the reiteration of the same behavior as in the first interaction but, of course, at a smaller scale. The last plot shows the two second-generation vortices which will again collide at some later time. This process eventually ends up with only one big stable vortex which moves toward the east among very small disturbances.

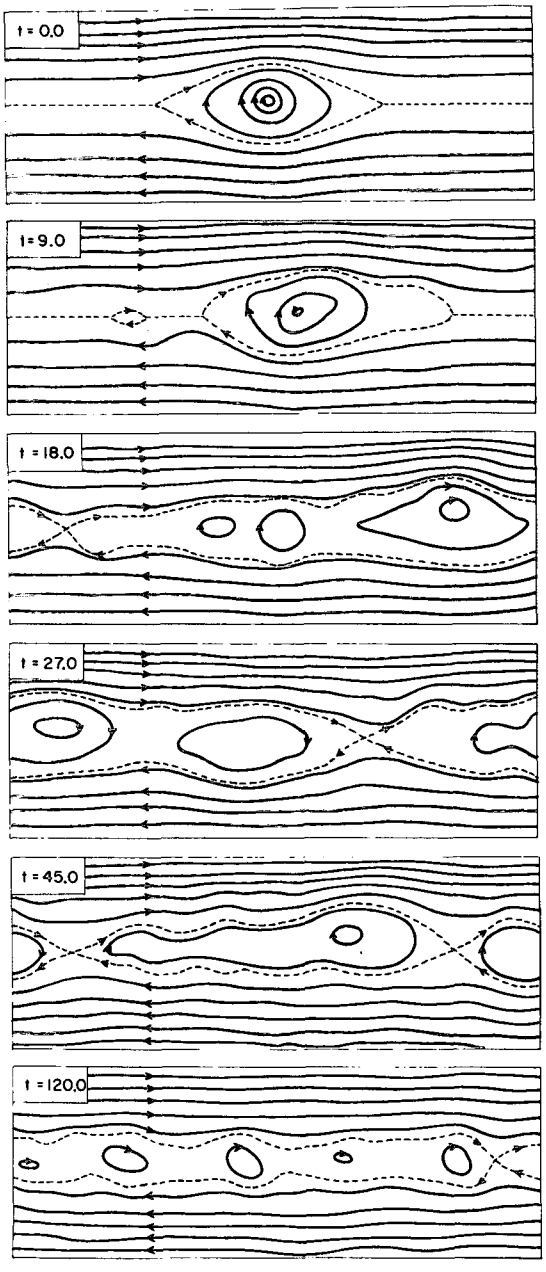

FIG. 6. An unstable solution for $k^2 = 2$, $P/K = 0.23$.

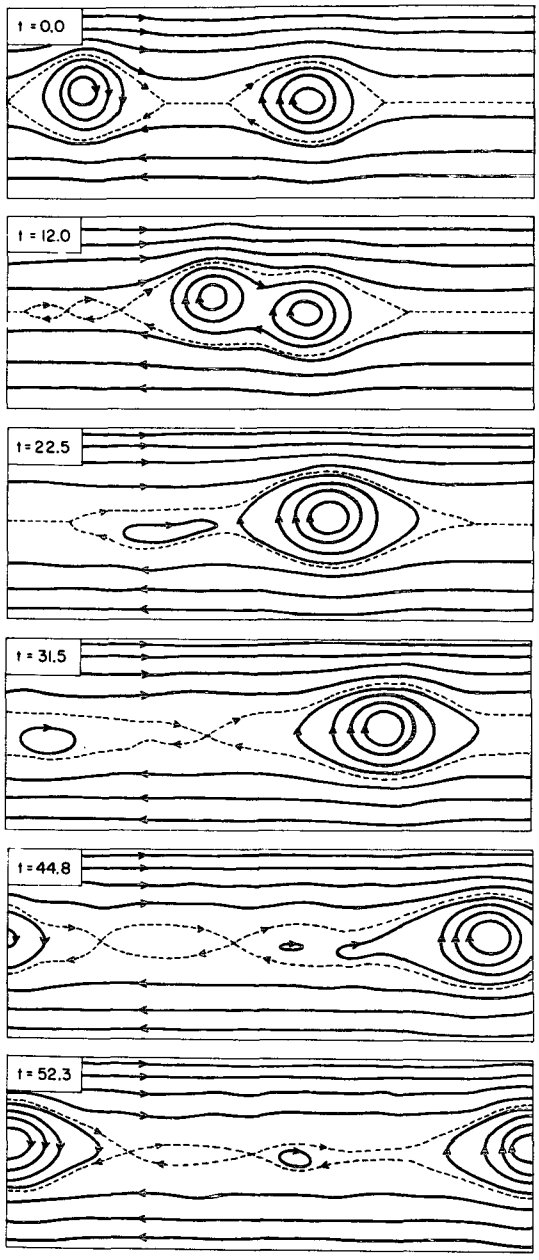

FIG. 7. Interaction of vortices for $k^2 = 10$. Because the solution is periodic in x, the two vortices that appear to be moving apart at $t = 22.5$ and $t = 31.5$ then collide, causing a smaller vortex to form at $t = 44.8$. Eventually, the large vortex sweeps up all the smaller vortices and the flow is steady.

Experiments also have been made in which a large number of vortices of equal size collide successively. After each collision the longitudinal size of the resulting vortex is substantially larger than that of the colliding vortices; the latitudinal size is only slightly larger.

This merging behavior is encouraging, for two reasons. First, it is in very good agreement with the imaging results from Voyager. To quote Smith *et al.*

(1979a), "Interactions between spots of equal size take place when the poleward member of a pair overtakes the other spot and combines with it. (Both spots are in an anticyclonic shear zone.) The combined mass tumbles for a while, and then usually ejects a streamer to the west and equatorward." Such observations are consistent with Fig. 7.

Second, the merging behavior suggests that a large vortex can sustain itself against a more realistic dissipative environment if it is fed frequently enough with small spots. This provides an alternate explanation for the longevity of features like the GRS. In the present inviscid model, such mechanism is not needed and its effect produces vortices of ever increasing size. The smaller spots on Jupiter may therefore be providing the energy, not only for the zonal jets, but also for the large, long-lived ovals. Presumably, these smaller spots get their energy directly from buoyancy. Whether this energy comes vertically from Jupiter's internal heat, or laterally from the sun's radiant heat, is still uncertain.

Acknowledgments. We thank Reta Beebe, Chris Bretherton, David Pollard, and Peter Rhines for useful comments in the early stages of this research. Judy Pechmann provided a critical review. The material was first presented at the Geophysical Fluid Dynamics Program at the Woods Hole Oceanographic Institution during the summer of 1980. The participants of that program gave helpful criticisms. The research was supported by the National Aeronautics and Space Administration, Planetary Atmospheres Program, under Grant NAGW-58. Contribution No. 3539 from the Division of Geological and Planetary Sciences, California Institute of Technology, Pasadena.

REFERENCES

Arakawa, A., 1966: Computational design for long-term numerical integration of the equations of fluid motion: Two-dimensional incompressible flow. Part 1. *J. Comput. Phys.*, **1**, 119–143.

Barcilon, A., and P. Gierasch, 1970: A moist, Hadley cell model for Jupiter's cloud bands. *J. Atmos. Sci.*, **27**, 550–560.

Beebe, R. F., A. P. Ingersoll, G. E. Hunt, J. L. Mitchell and J. P. Müller, 1980: Measurements of wind vectors, eddy momentum transports, and energy conversions in Jupiter's atmosphere from Voyager 1 images. *Geophys. Res. Lett.*, **7**, 1–4.

Flierl, G. R., V. D. Larichev, J. C. McWilliams and G. N. Reznik, 1980: The dynamics of baroclinic and barotropic solitary eddies. *Dyn. Atmos. Oceans*, **5**, 1–41.

Gierasch, P. J., A. P. Ingersoll and D. Pollard, 1979: Baroclinic instabilities in Jupiter's zonal flow. *Icarus*, **40**, 205–212.

Hatzes, A., D. D. Wenkert, A. P. Ingersoll and G. E. Danielson, 1981: Oscillations and velocity structure of a long-lived cyclonic spot. *J. Geophys. Res.*, **86**, 8745–8749.

Hide, R., 1963: On the hydrodynamics of Jupiter's atmosphere. *Mem. Soc. Roy. Sci. Leige, Ser. 5*, **7**, 481–505.

Holton, J. R., 1972: *An Introduction to Dynamic Meteorology*, 2nd ed. Academic Press, 391 pp. (see Chap. 4).

Ingersoll, A. P., 1969: Inertial Taylor columns and Jupiter's Great Red Spot. *J. Atmos. Sci.*, **26**, 744–752.

——, 1973: Jupiter's Great Red Spot: A free atmospheric vortex. *Science*, **182**, 1346–1348.

——, and J. N. Cuzzi, 1969: Dynamics of Jupiter's cloud bands. *J. Atmos. Sci.*, **26**, 981–985.

——, R. F. Beebe, S. A. Collins, G. E. Hunt, J. L. Mitchell, J. P. Müller, B. A. Smith and R. J. Terrile, 1979: Zonal velocity and texture in the Jovian atmosphere inferred from Voyager images. *Nature*, **280**, 773–775.

——, ——, J. L. Mitchell, G. W. Garneau, G. M. Yagi, and J. P. Müller, 1981: Interaction of eddies and mean zonal flow on Jupiter as inferred from Voyager 1 and 2 images. *J. Geophys. Res.*, **86**, 8733–8743.

Kuo, H. L., 1949: Dynamic instability of two-dimensional nondivergent flow in a barotropic atmosphere. *J. Meteor.*, **6**, 105–122.

Lin, C. C., 1955: *The Theory of Hydrodynamic Stability*. Cambridge University Press, 155 pp.

Lipps, F. B., 1965: The stability of an asymmetric zonal current in the atmosphere. *J. Fluid Mech.*, **21**, 225–239.

Maxworthy, T., and L. G. Redekopp, 1976: A solitary wave theory of the Great Red Spot and other observed features in the Jovian atmosphere. *Icarus*, **29**, 261–271.

Mitchell, T. L., R. F. Beebe, A. P. Ingersoll and G. W. Garneau, 1981: Flow fields within Jupiter's Great Red Spot and white oval BC. *J. Geophys. Res.* **86**, 8751–8757.

——, R. J. Terrile, B. A. Smith, J. P. Müller, A. P. Ingersoll, G. E. Hunt, S. A. Collins and R. F. Beebe, 1979: Jovian cloud structure and velocity fields. *Nature*, **280**, 776–778.

Pedlosky, J., 1979: *Geophysical Fluid Dynamics*. Springer-Verlag, 624 pp.

Redekopp, L. G., 1977: On the theory of solitary Rossby waves. *J. Fluid Mech.*, **82**, 725–745.

Reese, E. J., 1970: Jupiter's Red Spot in 1968–1969. *Icarus*, **12**, 249–257.

——, and B. A. Smith, 1968: Evidence of vorticity in the Great Red Spot of Jupiter. *Icarus*, **9**, 474–486.

Smith, B. A., and G. E. Hunt, 1976: Motions and morphology of clouds in the atmosphere of Jupiter. *Jupiter*, T. Gehrels, Ed., University of Arizona Press, 564–585.

——, L. A. Soderblom, T. V. Johnson, A. P. Ingersoll, S. A. Collins, E. M. Shoemaker, G. E. Hunt, H. Masursky, M. H. Carr, M. E. Davies, A. F. Cook II, J. Boyce, G. E. Danielson, T. Owen, C. Sagan, R. F. Beebe, J. Veverka, R. G. Strom, J. F. McCauley, D. Morrison, G. A. Briggs and V. E. Suomi, 1979a: The Jupiter system through the eyes of Voyager 1. *Science*, **204**, 951–972.

——, ——, R. F. Beebe, J. Boyce, G. A. Briggs, M. H. Carr, S. A. Collins, A. F. Cook II, G. E. Danielson, M. E. Davies, G. E. Hunt, A. P. Ingersoll, T. V. Johnson, H. Masursky, J. F. McCauley, D. Morrison, T. Owen, C. Sagan, E. M. Shoemaker, R. Strom, V. E. Suomi and J. Veverka, 1979b: The Galilean satellites and Jupiter: Voyager 2 imaging science results. *Science*, **206**, 927–950.

Stern, M. E., 1975: Minimal properties of planetary eddies. *J. Mar. Res.*, **33**, 1–13.

Stone, P. H., 1972: A simplified radiative-dynamical model for the static stability of rotating atmospheres. *J. Atmos. Sci.*, **29**, 405–418.

Williams, G. P., 1978: Planetary circulations: 1. Barotropic representation of Jovian and terrestrial turbulence. *J. Atmos. Sci.*, **35**, 1399–1426.

——, 1979: Planetary circulations: 2. The Jovian quasi-geostrophic regime. *J. Atmos. Sci.*, **36**, 932–968.